THE INFLUENCE OF AIRPLANE CONFIGURATION ON SONIC-BOOM CHARACTERISTICS

Harry W. Carlson

NASA Langley Research Center
Langley Station, Hampton, Va.

Presented at the AIAA-ASD Vehicle Design and Propulsion Meeting,
Dayton, Ohio,
November 4-6, 1963

THE INFLUENCE OF AIRPLANE CONFIGURATION ON SONIC-BOOM CHARACTERISTICS

Harry W. Carlson
Aerospace Engineer, Supersonic Mechanics Section
Full-Scale Research Division
Langley Research Center, NASA

Introduction

Sonic-boom considerations, which now impose serious operational restrictions on military supersonic airplanes, are certain to be of major concern in the development of future supersonic airplanes, particularly in regard to commercial supersonic air transports. Preliminary feasibility studies have indicated that boom considerations alone may dictate allowable minimum altitudes along most of the supersonic portion of the transport flight path and that in many cases the airframe sizing and engine selection may depend directly on the sonic-boom characteristics of the airplane. It is thus evident that final configuration selection for a supersonic transport will be influenced by these considerations.

It is the purpose of this paper to examine the dependence of sonic-boom overpressures on configuration variables and to point out, in general, design considerations which tend to minimize the problem. The study makes use of experimental data from wind-tunnel tests (refs. 1 to 4 as well as more recent data) and from the flight tests of reference 5. Theory derived from references 6 and 7 is used extensively in correlations with the measured data. The concept of a lower bound of sonic-boom overpressure, as discussed in references 8 and 9, is used in illustrating boom-minimization design considerations.

Symbols

A cross-sectional area of airplane or model determined by area-rule concepts

$A(t)$ nondimensionalized cross-sectional area, A/l^2, at nondimensionalized station $t = \frac{x}{l}$

$A_E(t)$ effective nondimensionalized cross-sectional area due to a combination of volume and lift effects, $A(t) + B(t)$

A_b cross-sectional area at base of airplane or model

B equivalent cross-sectional area due to lift at airplane or model station given by equation

$$B = \frac{\beta}{2q} \int_0^x F_L' \, dx$$

$B(t)$ nondimensionalized equivalent cross-sectional area due to lift, B/l^2, at nondimensionalized station $t = \frac{x}{l}$

$C_{D,o}$ drag coefficient at zero lift

C_L lift coefficient

F_L' lifting force per unit length along airplane or model longitudinal axis

$F(\tau)$ effective area distribution function, given by equation

$$F(\tau) = \frac{1}{2\pi} \int_0^\tau \frac{A_E''(t)}{\sqrt{\tau - t}} \, dt$$

h airplane flight altitude or lateral distance from model to measuring probe

K_r reflection factor

l length of airplane or model equivalent body

M Mach number

p reference pressure

Δp incremental pressure above or below ambient pressure due to flow field of airplane or model

q dynamic pressure

S wing planform area

t nondimensionalized distance measured along longitudinal axis from airplane or model nose, x/l

W airplane weight

ΔX distance along pressure signature from arbitrary reference point

α angle of attack, deg

$\beta = \sqrt{M^2 - 1}$

γ ratio of specific heats

τ dummy variable of integration measured in same direction and using same units as t

T_o value of τ giving the largest positive value of integral $\int_0^\tau F(\tau) d\tau$

x distance measured along longitudinal axis from airplane or model nose

μ Mach angle, $\sin^{-1} \frac{1}{M}$

Subscript:

max maximum

A prime (') is used to indicate a first derivative, and a double prime (") indicates a second derivative with respect to distance.

Discussion

A series of wind-tunnel tests treating several aspects of the sonic-boom problem have been conducted over a period of years in the Langley 4- by 4-foot supersonic pressure tunnel. Figure 1 shows a sketch of the apparatus used for the latter phases of the tests. The models (about 1 inch in length) were mounted on a sting support capable of remotely controlled changes in longitudinal position. Measurements of the model pressure field were made at each of three slender probes spaced across the tunnel at distances up to 50 inches. The dashed lines on the sketch represent a schematic diagram of the pressure instrumentation, which was a very critical part of the installation because it was required to measure with reasonable repeatability pressure differences as small as 0.05 psf. An inset sketch in figure 1 shows a typical measured pressure signature which displays a general N-shape. According to theory, supported by flight-test evidence, the pressure signature on the ground from an airplane in supersonic flight will have (except at extremely low altitudes) a sharp peaked N-shape similar to that shown by the dashed line in the sketch. Departures of the wind-tunnel measured pressure signature from a true sharp peaked N-shape wave are caused by the presence of near-field effects (double peak) and effects of vibration and probe boundary layer (rounded peaks). It has been found possible to adjust the tunnel data to compensate for these deficiencies simply by extending the linear portion of the measured curve and forming a right triangle whose area is equal to the area under the measured wave. Measured wind-tunnel bow-shock pressure rise Δp_{max}, as used throughout this paper, has been obtained from this adjusted signature. This adjustment was not applied in published results of earlier tunnel tests. A more detailed discussion of experimental apparatus and techniques may be found in reference 3.

The first use of the wind tunnel in sonic-boom work[1] was to explore some basic phenomena associated with thickness- and lift-generated flow fields. Figure 2 shows the measured pressure rise in parametric form plotted against the nondimensional distance from a non-axially-symmetric body having thickness but developing no lift. Although the overpressure measurements below the model and to the side are quite different at a distance of 1 body length, they become nearly equal at 8 body lengths, indicating an approach to flow-field axial symmetry. The pressure-rise parameter used herein has been derived from theory, a constant value of the parameter indicating the theoretical rate of decay of the pressure rise with distance, according to the three-quarter-power rule. A theoretical estimate of the pressure rise based on the distribution of normal cross-sectional areas along the body axis shows quite good agreement with the measured results. Actually, if area distributions based on $M = 2.0$ area-rule cuts were used, the theory would show that the flow field for non-lifting bodies without axial symmetry does not become truly axially symmetrical but only approximates that condition. This and other experimental investigations, both tunnel and flight tests, have established the validity of the equivalent-body concept in treating thickness-generated far-field pressures.

Large departures from axial symmetry of the flow field are shown for the lifting body of figure 3. As distance increases, the pressures above and below the wedge-section rectangular wing approach the attenuation, with distance expressed by the three-quarter-power rule (a constant value of the pressure-rise parameter). However, the magnitudes of the pressure rise above and below the wing are greatly different and show reasonable agreement with the far-field theory estimates.

The previous two figures have presented evidence of the ability of theoretical methods to estimate sonic-boom pressure rise for a body with thickness only and for a lifting body with thickness. Before proceeding further it will be advantageous to examine the means by which thickness (or volume) and lift effects are estimated and combined in the theory. Figure 4 presents an outline of the steps taken in estimating the pressure rise of the far-field bow shock directly below an airplane in level supersonic flight. The method shown here is in a form suitable for a numerical solution using desk calculators or electronic computing machines. It has been derived from the work of reference 7, the main differences stemming from changes in terminology and in the expression of lift effects in terms of equivalent cross-sectional area. The necessary inputs to the computation are a nondimensionalized airplane area distribution $A(t)$ formed by supersonic area-rule cutting planes $\left(\mu = \sin^{-1}\frac{1}{M}\right)$ and a nondimensionalized equivalent area distribution due to lift $B(t)$ evaluated, as indicated, through an integration of the lifting force per unit length along the airplane longitudinal axis. It is probable that increased precision results when the $A(t)$ curve includes areas under the boundary-layer displacement thickness and also accounts for the increase in area due to engine exhaust. The $B(t)$ curve is seen to depend on the weight of the airplane, the Mach number, and the dynamic pressure, in addition to the shape of the loading curve. A combined area distribution $A_E(t)$ is then formed by a direct addition of the $A(t)$ and $B(t)$ curves. The $A_E(t)$ curve is approximated by a series of parabolic arcs having a first derivative composed of connected straight-line segments and a second derivative composed of a step or pulse function. The integral involved in the $F(\tau)$ function can be evaluated quite easily when $A_E''(t)$ is a constant, and by superposition a complete $F(\tau)$ curve corresponding to the $A_E''(t)$ pulse distribution may be built up. An integration of the $F(\tau)$ function to the point T_o (hatched area on sketch) is then used in evaluating the pressure-rise characteristics expressed by the equation at the bottom of figure 4. The degree of approximation of the $A_E(t)$ curve can be improved by increasing the number of pulses used. In a machine-computing procedure using this technique, the airplane length is divided into 100 units.

A comparison of tunnel-measured bow-shock pressure rise at $M = 2$ for a complete airplane[3] with a theoretical estimate determined in the manner previously described is shown in figure 5. The theory curve is generated by repetition of the computational procedure for a series of values of the

lift parameter $\frac{\beta}{2} C_L \frac{S}{l^2}$. The area distribution A(t) used in the theory includes the estimated cross-sectional area under the displacement thickness of the laminar boundary layer assumed to exist on the small model. In this figure, the variation of the measured pressure-rise parameter with lift coefficient closely follows the theoretical estimate. As a matter of interest, theoretical curves are shown for the cases where volume effects alone or lift effects alone were considered. A notable feature of the data shown in figure 5 is that through a favorable combination of area and lift distributions the resultant overpressure becomes less than that associated with lift alone.

The ability of tunnel measurements and theory to provide reliable estimates of sonic-boom overpressure levels is illustrated in figure 6. Measured ground overpressures from flight tests of a supersonic bomber[5] are compared with estimates based on theory and on the tunnel test results shown in figure 5. Differences in area distributions due to estimated differences in model and airplane boundary layer are taken into account in making estimates based on tunnel data. A reflection factor of 2.0, corresponding to that measured for the dry lake bed of the flight tests, has been used in the estimates. The reference pressure was evaluated using the methods of reference 10. (It has been found that for a standard atmosphere a reasonable approximation to that value may be obtained simply by using the atmospheric pressure at midaltitude.) The agreement of measured and estimated overpressures is good, although there is a slight tendency toward underestimation.

It has been shown how the theory may be used to make reasonably reliable estimates of sonic-boom characteristics for specific configurations. The theory of references 6 and 7 has also made possible the definition of a lower bound of sonic-boom overpressure, which has been developed in references 8 and 9. Figure 7 serves to illustrate some of these lower-bound concepts. As shown previously, boom strength depends on an effective area distribution combining both volume and lift components. An example of an effective-area-distribution curve for an arrow-wing transport configuration is shown at the right of the figure. Note that the value of $A_E(t)$ at the base of the airplane is fixed by the airplane base area (including boundary-layer and engine-exhaust areas) and by the flight conditions of Mach number and lift coefficient. It has been found that the boom-strength parameter depends primarily on the value of the effective cross-sectional area at the base, but also depends on the shape of the complete $A_E(t)$ curve. In reference 8 the shape of the area-distribution curve yielding a minimum sonic boom was shown to be a function in which the area is proportional to the square root of the distance except in the immediate neighborhood of the airplane nose. Such a curve is shown by the dashed line on the right-hand side of figure 7. Thus, it is possible to write in simple equation form a lower bound of attainable sonic-boom overpressure that depends only on the airplane length, weight, base area, and flight conditions:

$$\frac{\left(\frac{\Delta p}{p}\right)_{max}\left(\frac{h}{l}\right)^{3/4}}{K_r \beta^{1/4}} = 0.54 \sqrt{\frac{\beta}{2} C_L \frac{S}{l^2} + \frac{A_b}{l^2}}$$

The method of approach used herein has followed that of reference 9, but the shape of the optimum area curve and the resultant shape factor of 0.54 were obtained from reference 8. The lower-bound expression neglects any minimum-volume restrictions and thus is inapplicable near zero lift coefficient. This has not proven to be a serious omission in the studies made to date. When volume restrictions become necessary they may be included, as was done in reference 9.

Theoretically, for a selected flight condition (a design point), it should be possible to redesign a configuration to approach, if not meet, the boom-minimization requirements. In the example shown in figure 7, the modification consisted of a tailoring of the fuselage area distribution, as shown by the dashed line. The overpressure characteristics of the original and modified configuration are shown on the left of the figure. Notice that the maximum theoretical reduction in boom strength (about 25 percent) occurs at the design point and that benefits fall off rapidly on either side of that point. In this example, the design point represents the transonic acceleration portion of the flight ($M = 1.4$, $h = 35{,}000$ feet). Whether any substantial portion of these benefits could be achieved in practice and whether the compromises with airplane design would be profitable are yet to be demonstrated.

Some experimental data felt to be applicable to the boom-reduction problem[4] are shown in figure 8. Measured and theoretical overpressures in parametric form have been plotted against a lift parameter for two wing-body models. The model with the wing in the rear location theoretically approaches the lower bound, even though it was not designed strictly in accordance with the concepts previously discussed. The experimental data however show only a part of the theoretical gains. Some of this discrepancy may be due to boundary-layer and separated-flow effects on the small models.

Of fundamental importance in any evaluation of configuration changes aimed at boom reduction is the resultant change in airplane drag. Figure 9 shows theoretical sonic-boom characteristics and corresponding values of zero-lift wave drag for an arrow-wing transport configuration and three modifications. The modifications consisted only of changes in fuselage area distribution. Configuration B, which was modified to approach the sonic-boom lower bound for a design point of $M = 3$ at an altitude of 60,000 feet, required a greatly enlarged forward fuselage with a resultant total airplane volume increase of 60 percent. This increase in volume resulted in an extremely large zero-lift drag penalty and also showed up as an increase in overpressure for zero lift. Configuration C with a design point of $M = 1.4$ at 35,000 feet had a total volume increase of 11 percent, but still showed a sizable drag penalty.

Configuration D was a compromise design, having no volume change, in which an attempt was made to produce a smooth effective-area-distribution curve (similar to that of the area distribution for a minimum-wave-drag body of revolution) for the design point of $M = 3$, $h = 60{,}000$ feet. The decrease in overpressure, which was not so pronounced as for the other two modifications, extended over the whole range of lift coefficients, and only a small drag penalty was shown. There are, of course, so many other factors involved which have not been studied that it is impossible at this time to draw any conclusions regarding the feasibility of these boom-minimization concepts.

An interesting comparison of the sonic-boom characteristics of two transport configuration models is shown in figure 10. Both theoretical and experimental data are shown and are compared with the lower bound. Cross-sectional areas used in the theory include area within the estimated displacement thickness of a laminar boundary layer. The lower overpressures for the arrow-wing design may be attributed to the reduced base area and to smooth area- and lift-distribution curves. Estimated ground overpressures for these configurations sized to accommodate 125 passengers (take-off weight of 400,000 pounds) are shown in figure 11. A reflection factor of 1.9 was assumed, and the reference pressure was taken as the standard atmosphere pressure at midaltitude. A weight of 360,000 pounds at a Mach number of 1.4 was chosen to represent the critical climb portion of the flight, and a weight of 300,000 pounds at a Mach number of 3 was chosen to represent the cruise portion. For a cruise altitude of 70,000 feet, the canard design would have an overpressure of about 1.6 psf compared with 1.4 psf for the arrow-wing design. In view of the many compromises involved, it is believed that a practical boom-optimized airplane would not be able to achieve the corresponding lower-bound value of 1.15 psf, and that attainable minimum overpressures are likely to be nearer to the 1.4 psf level. Any reduction in airplane weight would, of course, be beneficial, the overpressure being roughly proportional to the square root of the weight.

Concluding Remarks

Both wind-tunnel and flight tests have demonstrated conclusively that both volume and lift effects contribute to bow-shock overpressures. Experiment has shown that existing theory provides reasonably accurate estimates of overpressure, both for cases of thickness (or volume) alone and for a combination of thickness and lift. Additional developments of the theory have made possible the definition of a lower bound of sonic-boom overpressure which depends only on airplane length, weight, base area (including jet-exhaust and wake effects), and flight conditions. A corollary of the lower-bound concept provides airplane design methods that theoretically allow lower-bound overpressure values to be achieved. However, one preliminary experiment has indicated that this lower bound may not be actually realized. It has also been indicated that compromises with other design considerations will prevent anything more than a limited approach to lower-bound overpressures.

References

1. Carlson, Harry W.: An Investigation of Some Aspects of the Sonic Boom by Means of Wind-Tunnel Measurements of Pressures About Several Bodies at a Mach Number of 2.01. NASA TN D-161, 1959.

2. Carlson, Harry W.: An Investigation of the Influence of Lift on Sonic-Boom Intensity by Means of Wind-Tunnel Measurements of the Pressure Fields of Several Wind-Body Combinations at a Mach Number of 2.01. NASA TN D-881, 1961.

3. Carlson, Harry W.: Wind-Tunnel Measurements of the Sonic-Boom Characteristics of a Supersonic Bomber Model and a Correlation With Flight-Test Ground Measurements. NASA TM X-700, 1962.

4. Morris, Odell A.: A Wind-Tunnel Investigation at a Mach Number of 2.01 of the Sonic-Boom Characteristics of Three Wing-Body Combinations Differing in Wing Longitudinal Location. NASA TN D-1384, 1962.

5. Hubbard, Harvey H., Maglieri, Domenic J., Huckel, Vera, and Hilton, David A.: Ground Measurements of Sonic-Boom Pressures for the Altitude Range of 10,000 to 75,000 Feet. NASA TM X-633, 1962.

6. Whitham, G. B.: The Behaviour of Supersonic Flow Past a Body of Revolution, Far From the Axis. Proc. Roy. Soc. (London), ser. A, vol. 201, no. 1064, March 7, 1950, pp. 89-109.

7. Walkden, F.: The Shock Pattern of a Wing-Body Combination, Far From the Flight Path. Aero. Quarterly, vol. IX, pt. 2, May 1958, pp. 164-194.

8. Jones, L. B.: Lower Bounds for Sonic Bangs. Jour. R.A.S., vol. 65, June 1961, pp. 433-436.

9. Carlson, Harry W.: The Lower Bound of Attainable Sonic-Boom Overpressure and Design Methods of Approaching This Limit. NASA TN D-1494, 1962.

10. Friedman, Manfred P., Kane, Edward J., and Sigalla, Armand: Effects of Atmosphere and Aircraft Motion on the Location and Intensity of a Sonic Boom. AIAA Jour., vol. 1, no. 6, June 1963, pp. 1327-1335.

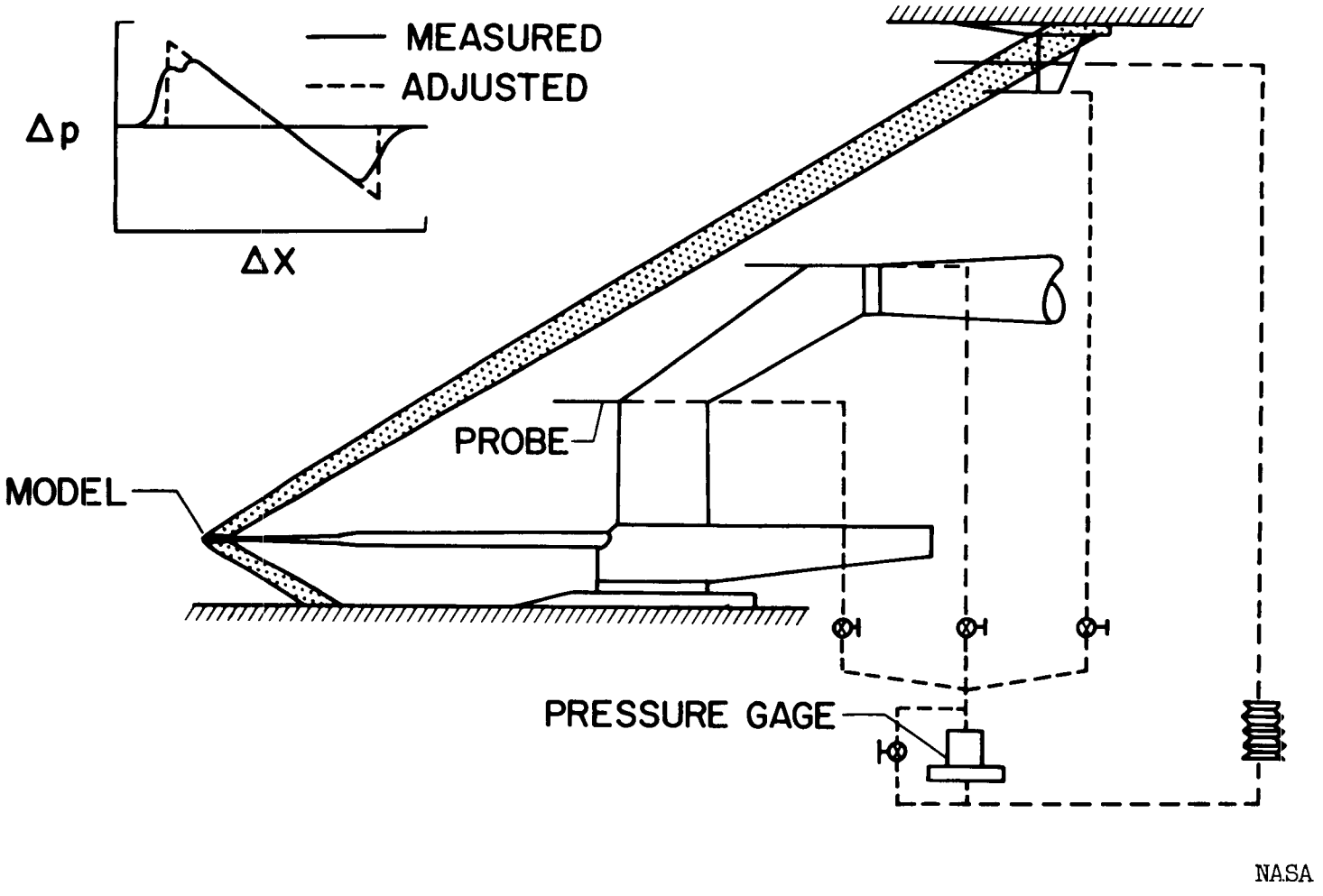

Figure 1.- Tunnel test apparatus and typical measured pressure signature.

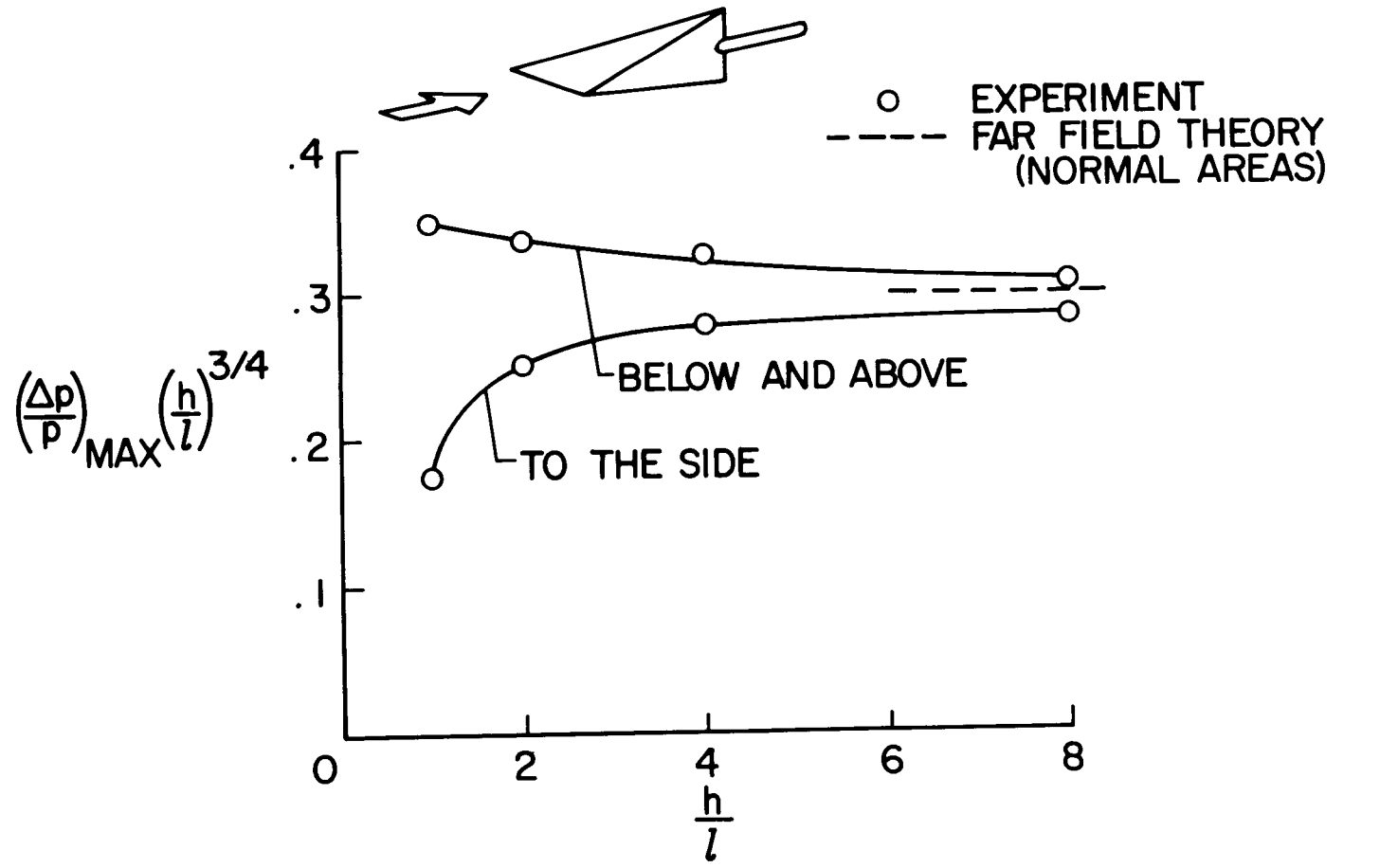

NASA

Figure 2.- Tunnel measurements of thickness-induced pressure field.

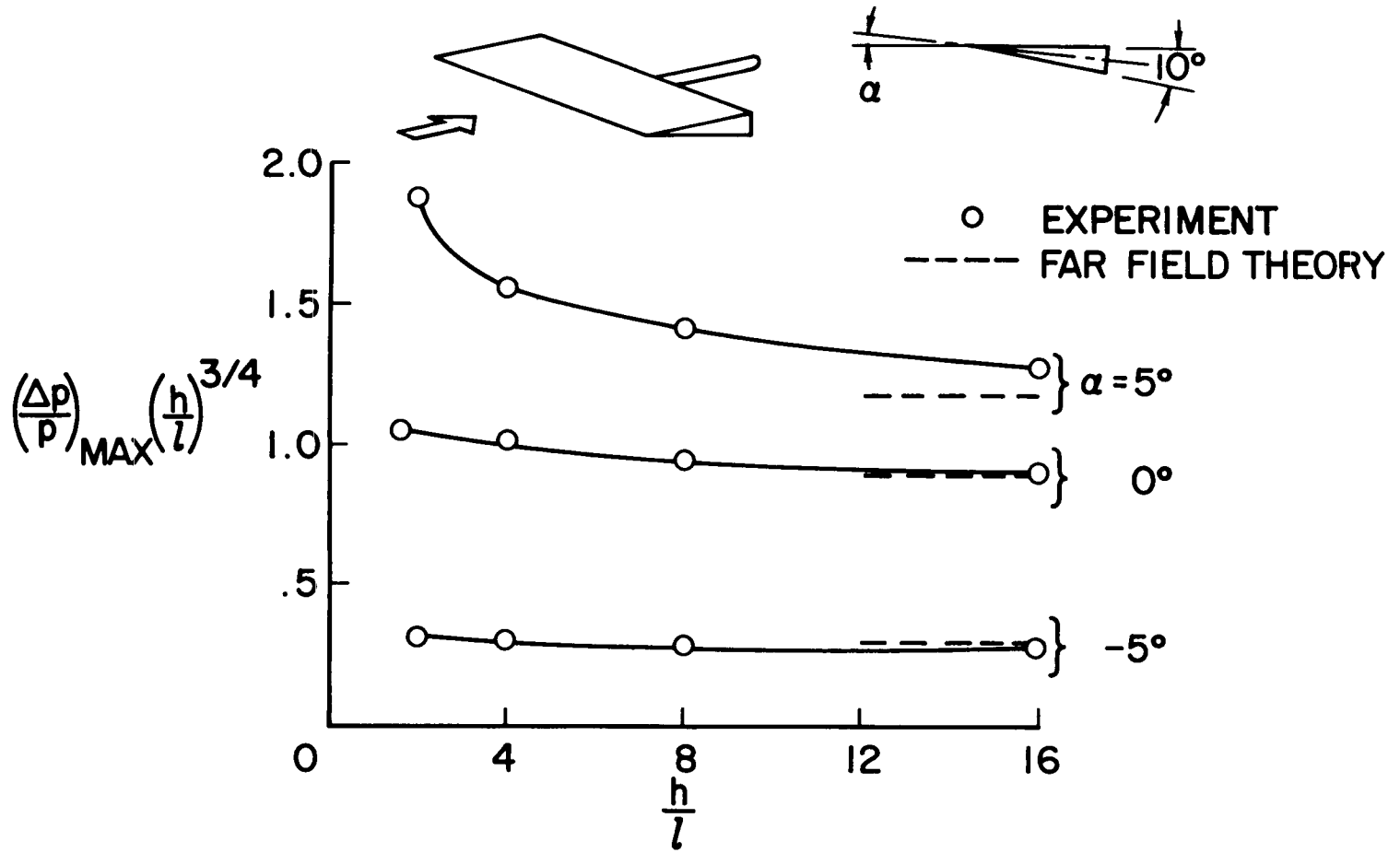

NASA

Figure 3.- Tunnel measurements of lift-induced pressure field.

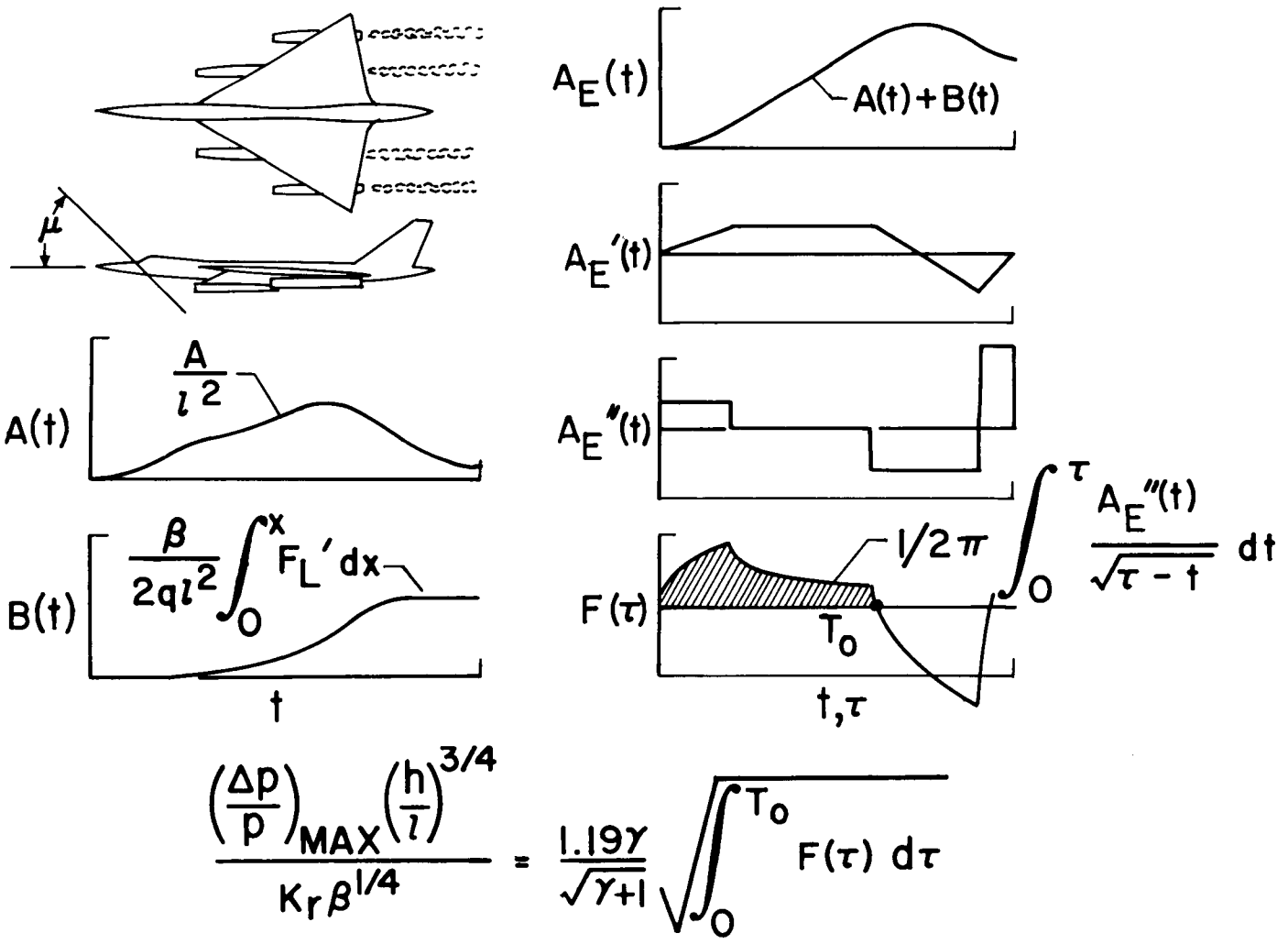

NASA

Figure 4.- Outline of steps in theoretical estimation method.

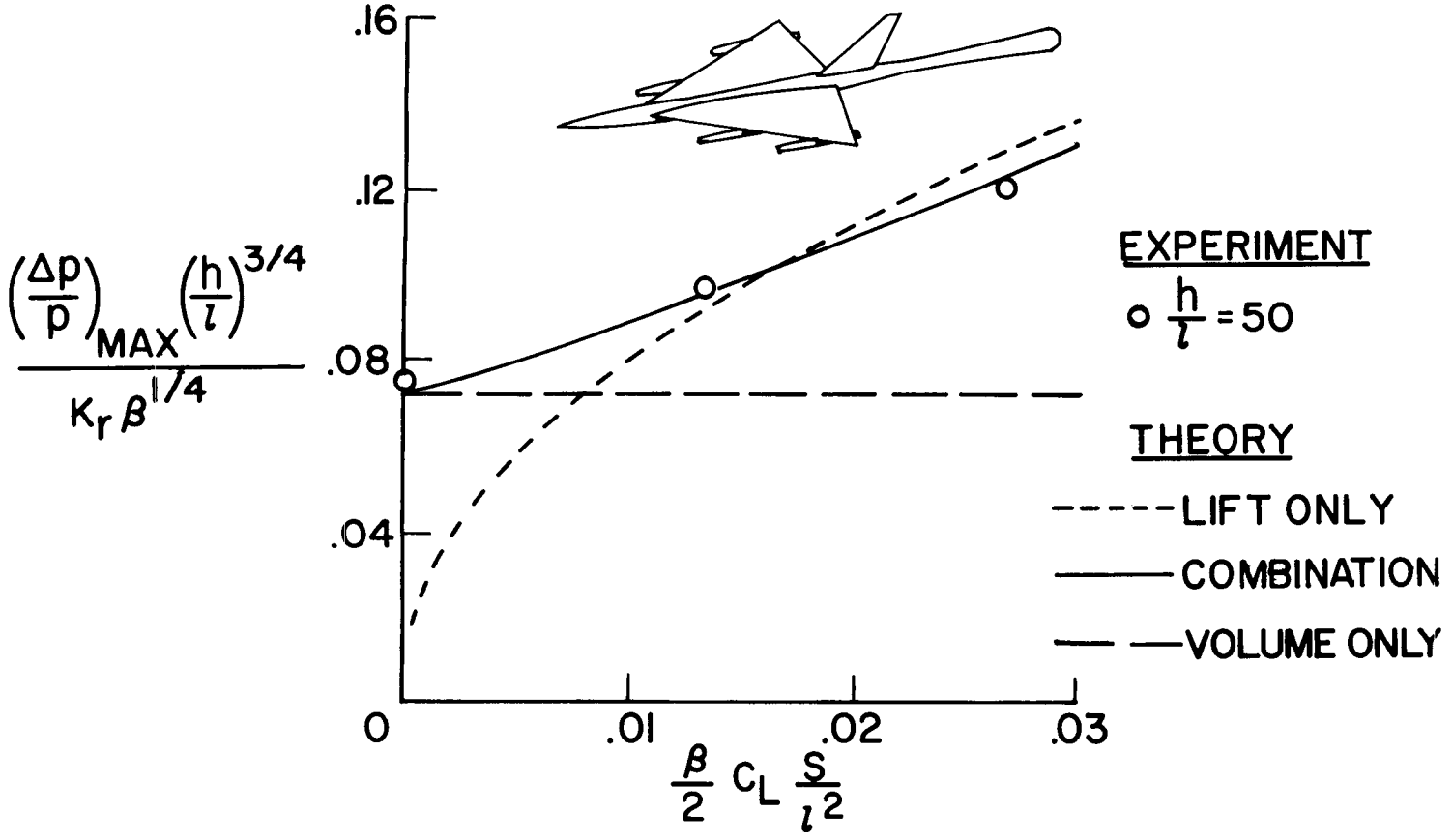

NASA

Figure 5.- Tunnel measurements of pressure field below an airplane model, M = 2.

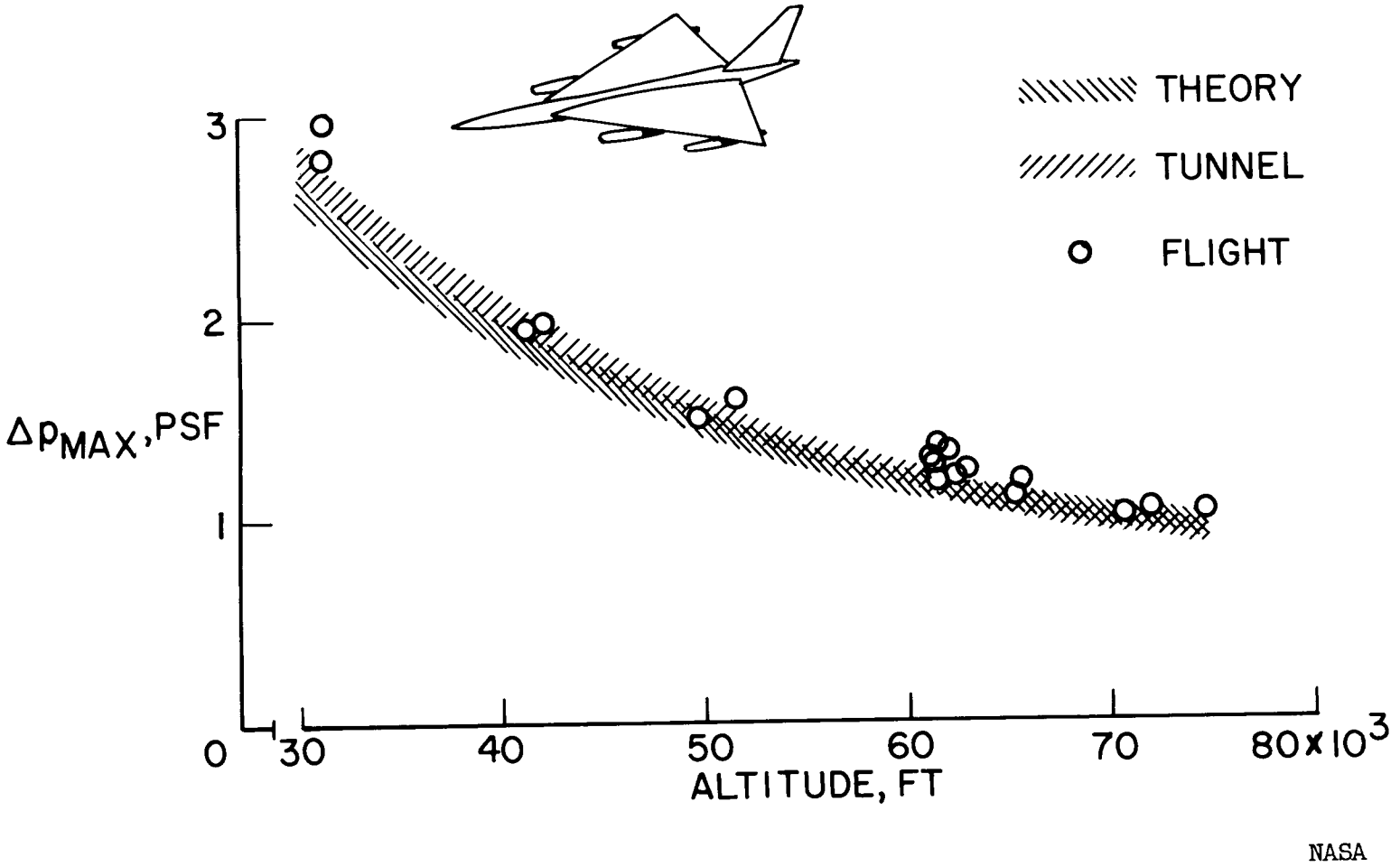

Figure 6.- Correlation of tunnel data, flight data, and theory.

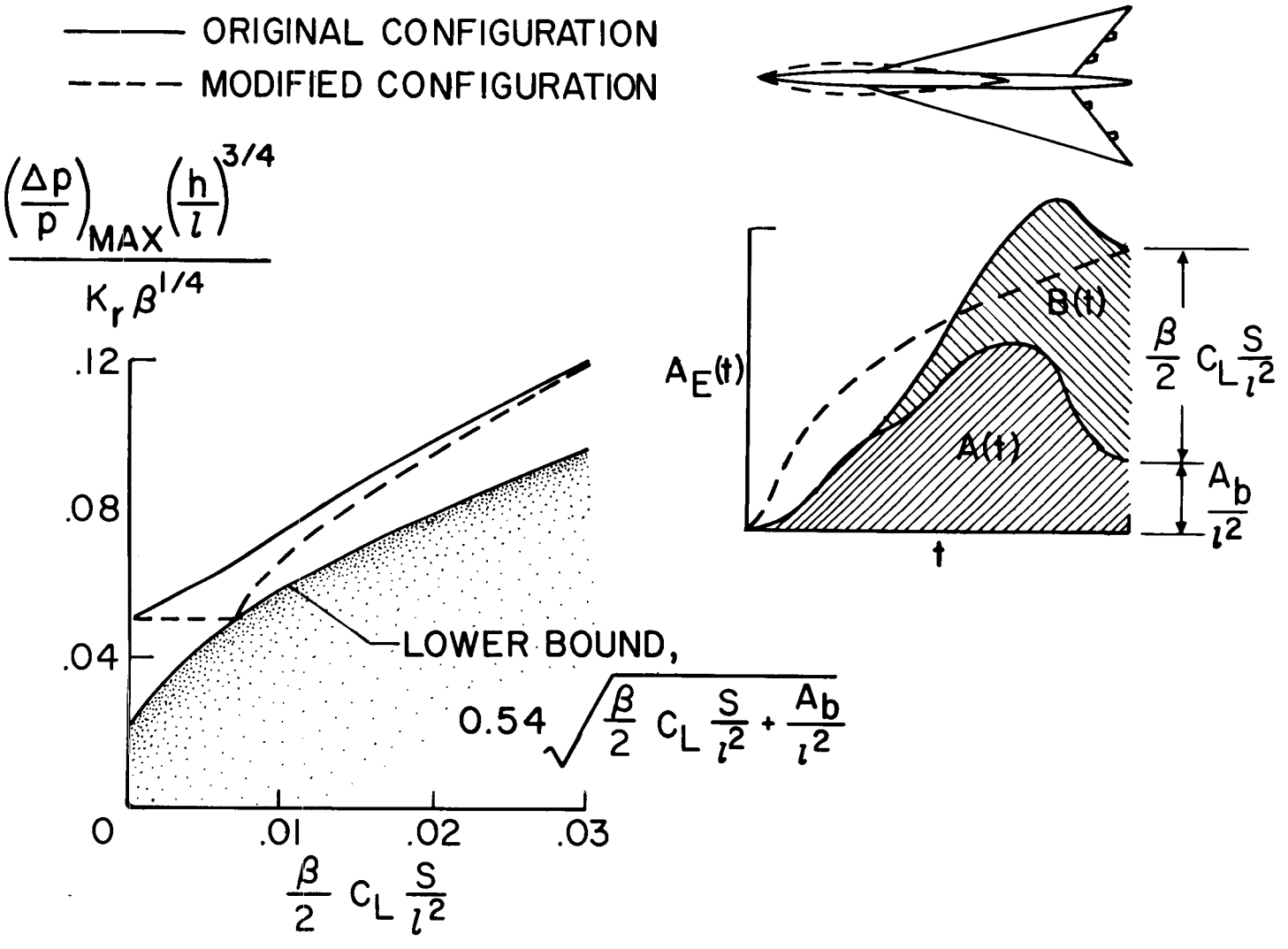

NASA

Figure 7.- Theoretical considerations for configuration sonic-boom optimization.

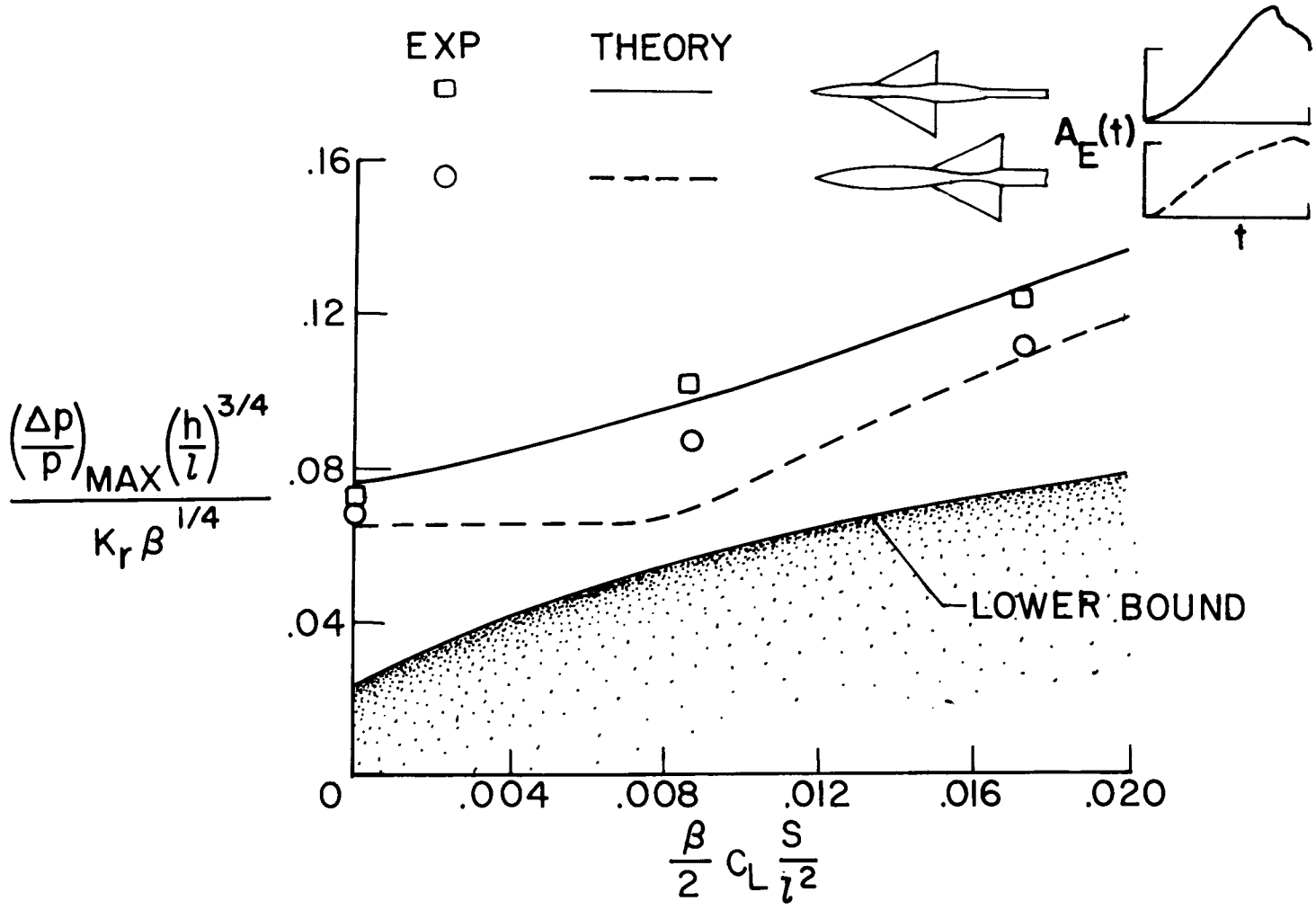

NASA

Figure 8.- Experimental study of configuration effects.

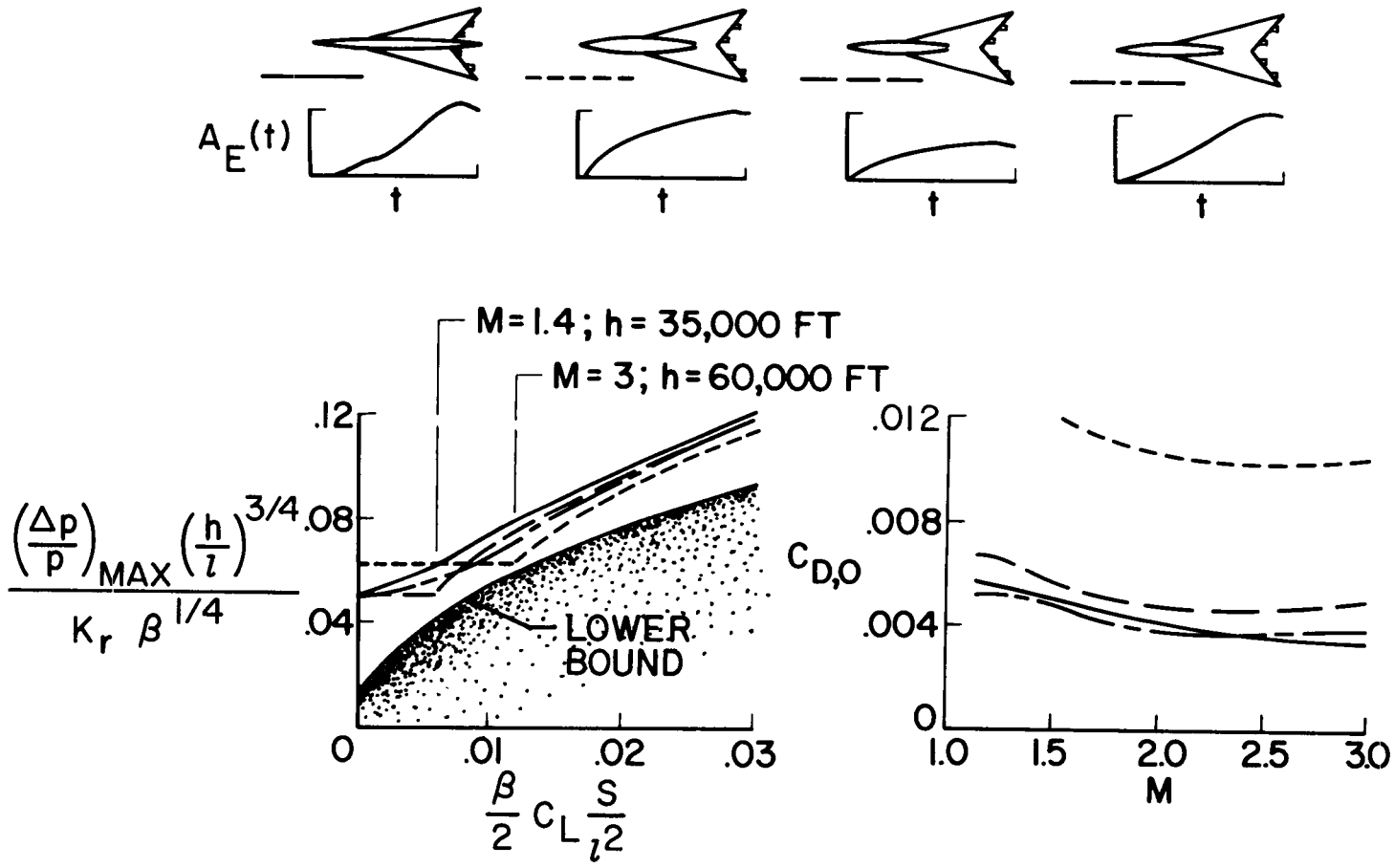

NASA

Figure 9.- Overpressure-drag relationship for boom optimized configurations.

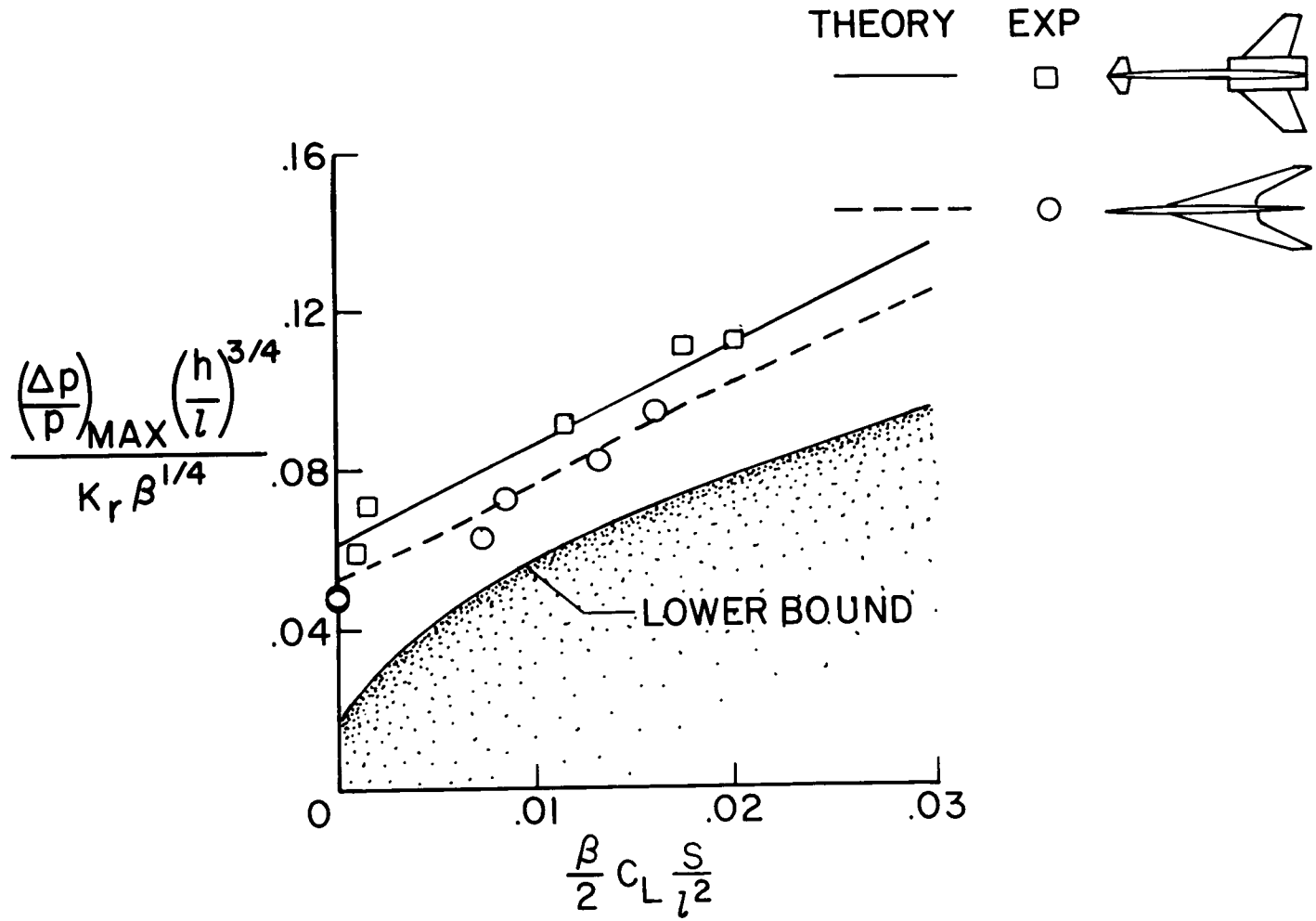

NASA

Figure 10.- Experimental sonic-boom characteristics for two transport configurations, M = 1.4 and 2.

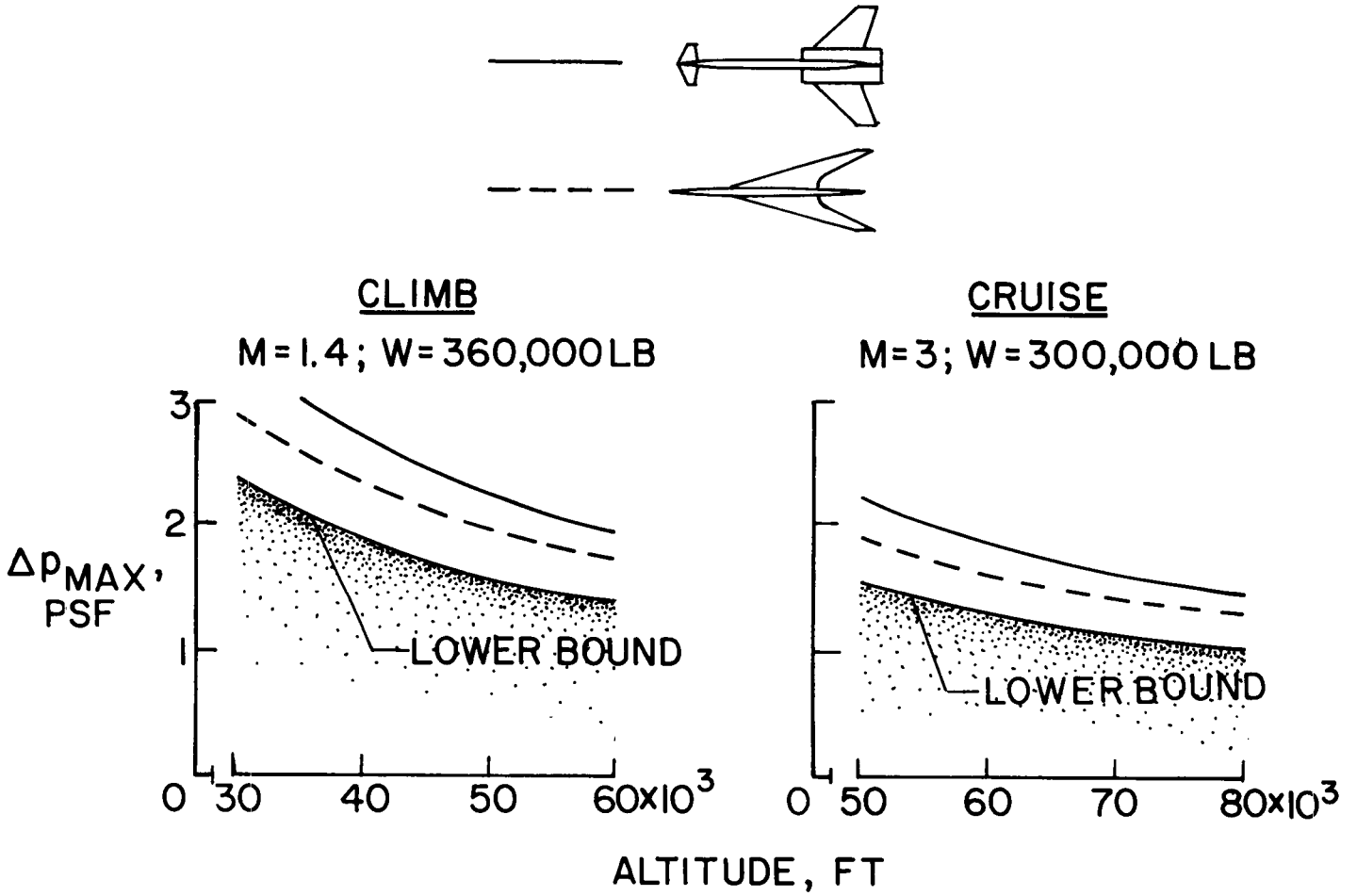

NASA

Figure 11.- Estimated ground overpressures for two transport configurations.